☙

Mott insulator to metal transition in filling-controlled SmMnAsO$_{1-x}$

Y. Shiomi,[1,2] S. Ishiwata,[1,3] Y. Taguchi,[2,3] and Y. Tokura[1,2,3,4]

[1]*Department of Applied Physics, University of Tokyo, Tokyo 113-8656, Japan*
[2]*Cross-Correlated Materials Research Group (CMRG), RIKEN Advanced Science Institute, Wako 351-0198, Japan*
[3]*Correlated Electron Research Group (CERG), RIKEN Advanced Science Institute, Wako 351-0198, Japan*
[4]*Multiferroics Project, ERATO, Japan Science and Technology Agency (JST), Tokyo 113-8656, Japan*

Transport and magnetic properties have been systematically investigated for SmMnAsO$_{1-x}$ with controlled electron doping. As the electron band filling is increased with the increase of oxygen deficiency (x), the resistivity monotonically decreases, and the transition from Mott-insulator to metal occurs between $x = 0.17$ and 0.2. The Seebeck coefficient at room temperature abruptly changes around the critical doping level from a large value ($\sim -300\ \mu$V/K) to a small one ($\sim -50\ \mu$V/K) both with negative sign. In the metallic compounds with $x = 0.2$ and 0.3, Mn spins order antiferromagnetically around 30 K, and the Hall coefficient with the negative sign shows a reduction in magnitude upon the magnetic transition, indicating the change in the multiple Fermi surfaces. A gigantic positive magnetoresistance effect is observed in a wide range of temperatures, reaching up to 60% at 2 K for the $x = 0.3$ compound. The effect is attributed to the field-induced change of the complex Fermi surfaces in this multiorbital correlated electron system.

I. INTRODUCTION

Since the recent discovery of superconductivity in doped LaFeAsO[1,2] and related materials with high transition critical temperatures, the Fe-based layered pnictides have attracted much interest similarly to the cuprate superconductors. The crystal structure of the parent material RFeAsO (R stands for a rare-earth metal) is classified into ZrCuSiAs type (space group $P4/nmm$). Up to now, more than 70 materials with $RMP n$O formula (where M is a transition metal and Pn is a pnictogen) have been known to have this crystal structure. The presence of such a large number of materials is due to the fact that the substitution of many other $3d$ or $4d$ transition metals is possible for an M site in addition to rich variation in Pn sites (P, As, Sb, and Bi) and R sites (La-Dy).[3] In this crystal structure, an insulating $(R^{3+}O^{2-})^{+}$ layer and a conducting $(M^{2+}Pn^{3-})^{-}$ layer are alternatingly stacked along the c axis. As an example, the structure of SmMnAsO is depicted in Fig. 1(a). In the $(Sm^{3+}O^{2-})^{+}$ layer, O^{2-} is tetrahedrally coordinated by Sm^{3+} ions. The $(Mn^{2+}As^{3-})^{-}$ layer also has the same connectivity of the ions, but the cation and anion are interchanged.

The physical properties of the compounds LaMPnO ($M =$ Mn, Co, and Ni, $Pn =$ P and As) have been extensively studied by Hosono and coworkers.[4] According to their study, LaMnPO is an antiferromagnetic insulator with an optical gap larger than 1 eV and high Néel temperature (above 375K). LaCoPO and LaCoAsO are ferromagnetic metals with $T_c = 43$ and 70 K, respectively. LaNiPO and LaNiAsO are paramagnetic metals and show superconductivity in the low-temperature region (<3 K). For LaMnPO, Yanagi $et\ al.$ synthesized a bulk polycrystalline sample and investigated the physical properties.[5] The resistivity is ~ 1 kΩcm around room temperature and shows insulating temperature dependence, which well obeys the Arrhenius-type relation.[5] A neutron powder diffraction measurement indicates that the moment of Mn^{2+} ($3d^5$) spin is $2.26\mu_B$, which is smaller than $5\mu_B$/Mn expected for the high-spin state ($S = 5/2$), and that the Mn spins within the MnP layer show antiparallel arrangement and

parallel arrangement along the c axis at room temperature. Quite recently, RMnPO with other rare-earth elements ($R =$ Nd, Sm, and Gd) were also investigated.[6] The resistivity at room temperature is about three orders of magnitude smaller than that of LaMnPO, but the temperature dependence remains semiconducting. Magnetization measurements indicate that Mn^{2+} spins order antiferromagnetically, and that the T_N is higher than 350 K, similarly to LaMnPO. Concerning LaMnAsO, Kayanuma $et\ al.$[7] synthesized an epitaxially grown film with a small amount of impurity (LaMnO$_3$). The resistivity is ~ 1 Ωcm at room temperature, although a relatively large charge gap of ~ 1 eV is predicted by the band calculations.[7] This material is also considered as an antiferromagnetic insulator analogous to LaMnPO,[4] yet the magnetic property has not been reported.

For RFeAsO, R-dependent physical properties have been intensively investigated in which the superconducting transition temperature of doped materials depends significantly on the R species.[8] In the case of $M =$ Co, Ohta and Yoshimura[9] recently investigated the magnetism of the RCoAsO ($R =$ La-Gd), and showed that the antiferromagnetic state is more stable than the ferromagnetic state in the compounds with relatively small R ions. On the other hand, there have been few reports on RMnAsO with other rare earth element than $R =$ La and their physical properties are hardly unveiled. Recently, Marcinkova $et\ al.$ reported the magnetic property of NdMnAsO,[10] which is an antiferromagentic semiconductor with $T_N = 359$ K. Neutron powder diffraction measurements showed that, below T_N, Mn^{2+} spins order antiferromagnetically pointing along c axis with the same spin-ordering pattern as in LaMnPO. With further cooling, the Mn^{2+} spins show reorientation, lying within the ab plane at $T_{SR} = 23$ K, accompanied by the antiferromagnetic order of Nd^{3+} moments. Across the spin-reorientation transition, the ordering pattern of Mn^{2+} spins remains unchanged. Nd^{3+} moments align ferromagnetically within a NdO layer antiferromagnetically along the perpendicular direction.
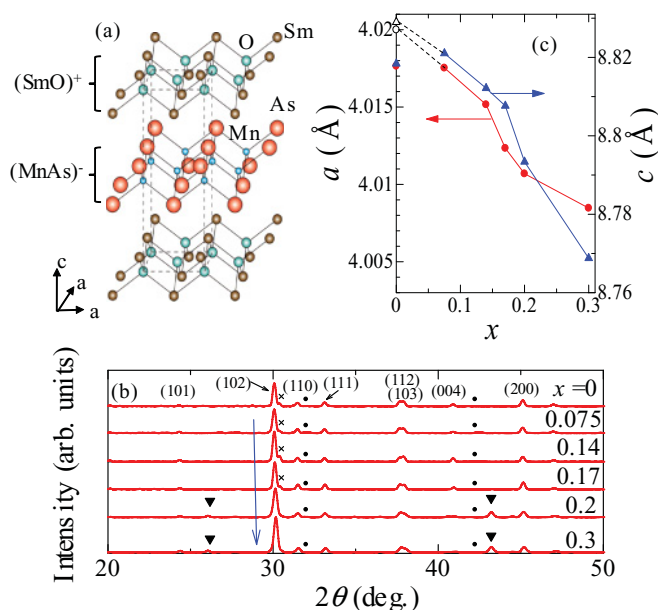
FIG. 1. (Color online) (a) Schematic diagram of the crystal structure of SmMnAsO. Dashed lines show the tetragonal unit cell. (b) Powder x-ray diffraction patterns for $x = 0$–0.3. Cross marks indicate unknown impurity peaks. The closed triangles and circles denote the SmAs peaks and the expected peak positions of MnAs, respectively. (c) Lattice constants (a and c) are plotted against nominal oxygen deficiency (x).

A promising way to find the emergent phenomena in such electron-correlated materials is the band-filling (doping) control, which has been extensively adopted in the past decades,[11] and is also the main focus of the present paper. In RMnPO, the hole doping by substitution of R (La, Nd, Sm, and Gd) with Ca or Cu below 10% was reported.[5,6] While undoped RMnPO shows n-type conduction, the Ca- or Cu-doped samples have p-type carrier as judged from the Seebeck coefficient. The resistivity for the doped samples decreases in magnitude, but the temperature dependence remains semiconducting. In this paper, we demonstrate that doping a large amount of electrons is possible for a Mn-based oxy-arsenide SmMnAsO$_{1-x}$ by introducing oxygen deficiency (x) with the use of high-pressure synthesis technique. The undoped SmMnAsO is a Mott-insulator, and the insulator-metal transition occurs at $x = 0.2$. The metallic samples ($x = 0.2$ and 0.3) show antiferromagnetic transition at around 30K, and the Hall coefficient shows a reduction upon the transition. These metallic state exhibits unconventionally large positive magnetoresistance up to 60% at 2 K under 9 T. The Seebeck coefficient with negative sign changes from a large absolute value arising from variable-range-hopping (VRH) conduction to a metallic small one upon the insulator-metal transition as a function of the oxygen deficiency ($x \sim 0.2$), ensuring the bulk nature of the transition.

II. EXPERIMENT

First, SmAs was prepared as a precursor by sintering Sm (3N, shot) and As (5N, powder) at 1050 °C for 24 h in an evacuated silica tube. SmMnAsO samples with controlled oxy-

gen deficiency (SmMnAsO$_{1-x}$) were made by high-pressure synthesis technique with the use of a cubic anvil press. SmAs, Mn (3N, powder), and MnO (3N, powder) were mixed in a prescribed ratio ($\sim$0.2 g) in an Ar-filled glove box and fired at 1150 °C for 1 hour under 6.5 GPa in a BN crucible. The products were examined with powder x-ray diffraction. The resistivity, Hall resistivity, and specific heat were measured by using a physical property measurement system (by Quantum Design). The magnetoresistance was measured in the longitudinal configuration, i.e., the magnetic field parallel to the electric current. Seebeck coefficient and thermal conductivity were measured with a conventional steady-state method. Magnetization measurement was performed by using a SQUID magnetometer, magnetic property measurement system (by Quantum Design).

III. RESULTS AND DISCUSSIONS

A. Sample characterization

High-pressure synthesis technique enabled us to obtain the oxygen-deficient samples up to $x = 0.3$. Figure 1(b) shows the x-ray diffraction patterns for these materials. Almost single-phase samples were obtained up to $x = 0.17$, but for $x = 0.2$ and 0.3, the products contained a small amount (less than 4% in volume fraction) of SmAs as an impurity (indicated by closed triangles). Also, the presence of a tiny amount of ferromagnetic impurity, MnAs, was indicated by the magnetization measurement (2–6% for $x \leqslant 0.17$ and below 0.5% for $x \geqslant 0.2$) although hardly identified by the powder x-ray diffraction [expected peak positions for MnAs are indicated by closed circles in Fig. 1(b)]. Figure 1(c) shows the obtained lattice constants (a and c) for these samples. The open circle and triangle indicate the reported values for the $x = 0$ compound synthesized by a different method.[3] In the present sample preparation condition, the c value of $x = 0$ is smaller than that of $x = 0.075$. It appears that the obtained samples contain more oxygen than the nominal value and the stability of Sm$_2$O$_3$ phase prevents the synthesis of the compound without oxygen deficiency. One possible reason might be the slight oxidization of Sm during the synthesis in the evacuated silica tube. Above $x = 0.075$, the lattice constants decrease monotonically with increasing x, similarly to RFeAsO$_{1-x}$.[8] Among all the samples synthesized in the present work, the $x = 0.075$ has the largest lattice constants. Since the lattice constants for $x = 0.075$ are smaller than the reported values for $x = 0$, the present $x = 0.075$ compound is considered to be slightly oxygen deficient. We tried to synthesize the compounds with larger lattice constants than $x = 0.075$, but could not obtain such a sample. On the other hand, the sample with nominal value of $x = 0$ shows similar lattice constants with $x = 0.075$ compound. This sample probably contains slight excess oxygen, in accord with the presence of carriers, which is indicated by the downturn of resistivity around 50 K (data not shown).

B. Resistivity and Seebeck coefficient

Figure 2(a) shows the temperature (T) dependence of the resistivity (ρ) for all the samples. For $x = 0.075$, the temperature dependence of the resistivity is insulating and
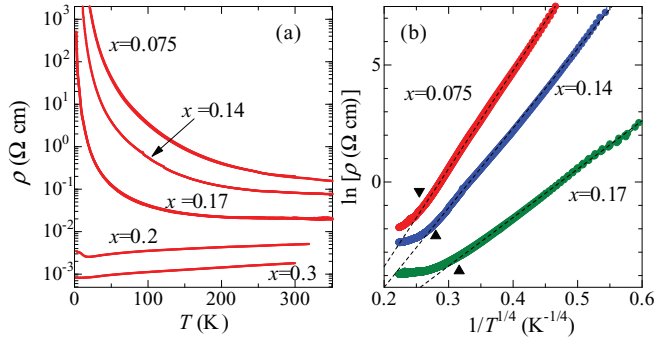
FIG. 2. (Color online) (a) Temperature (T) dependence of resistivity (ρ). (b) Resistivity for the insulating samples plotted in the form of variable-range-hopping (VRH) relation in three dimensions. The dashed lines are linear fits to the data. The triangles indicate the temperature at which the VRH conduction sets in (T_{VRH}).

increases rapidly with decreasing temperature. It was reported for NdMnAsO that the resistivity increases with decreasing temperature above 250 K, but tends to decrease below that temperature.[10] In contrast to such complex temperature-dependence in NdMnAsO, the resistivity of SmMnAsO$_{1-x}$ with $x = 0.075$ seems to show a simple insulating behavior like LaMnPnO (Pn = P, As, or Sb).[7] As x is increased, the resistivity decreases monotonically, but shows the insulating temperature dependence up to $x = 0.17$. The temperature dependence of resistivity for $x = 0.075$, 0.14, and 0.17 samples does not follow the thermal-activation-type relation,

$$\ln \rho(T) \propto E_0/k_B T, \qquad (1)$$

but well obeys the variable-range-hopping (VRH) relation in three dimensions, as exemplified in Fig. 2(b). The Mott's VRH relation is given by

$$\ln \rho(T) \propto (T_0/T)^{1/4}, \qquad (2)$$

where T_0 depends inversely on the localization length and the density of localized states at the Fermi energy. The apparent three-dimensional conduction observed in the present samples may indicate that the interlayer hopping is substantial in this temperature range despite the layered structure. The slope of the line in Fig. 2(b) (which is equal to $T_0^{1/4}$) decreases with increasing x, indicating that the localization length becomes longer and/or the density of localized states increases. The temperatures where the resistivity deviates from the VRH conduction (T_{VRH}) are indicated by black triangles in Fig. 2(b).

As the doping proceeds to $x = 0.2$, the temperature dependence of the resistivity changes to a metallic behavior. For $x = 0.2$, the resistivity decreases with decreasing temperature down to 20 K, but it turns to increase at around that temperature. As will be discussed later, the antiferromagnetic transition of the Mn spins is observed at 27 K, which is slightly higher than the temperature of the resistivity upturn [see also Fig. 8(a)]. The resistivity upturn is probably due to the change in the Fermi-surface shape and/or spin-dependent renormalization of transfer interaction upon the antiferromagnetic or spin-density-wave (SDW) transition of Mn electrons. Another possibility would be the Anderson localization in this polycrystalline sample with the disorder (oxygen deficiency), but this possibility would be ruled out from the result of
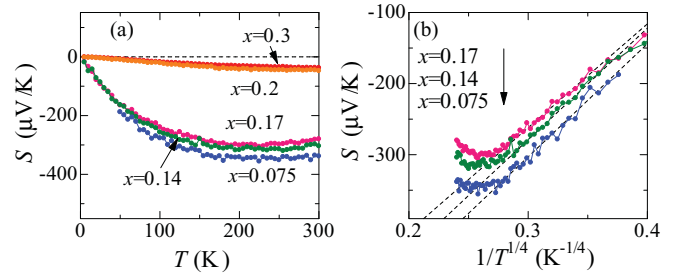

FIG. 3. (Color online) (a) Temperature (T) dependence of the Seebeck coefficient (S). (b) Seebeck coefficients of insulating samples are plotted in the form of S vs $1/T^{1/4}$.

magnetoresistance (*vide infra*). The resistivity upturn is not observed for $x = 0.3$ down to 2 K and the value is comparable with that of superconducting RFeAsO$_{1-x}$.[8] While the residual resistivity is less than 1 mΩcm, the superconductivity is not observed above 0.35 K.

Figure 3 shows the Seebeck coefficients of all the samples. As shown in Fig. 3(a), the Seebeck coefficient (S) exhibits quite a different behavior between the insulating ($x = 0.075$, 0.14, and 0.17) and the metallic ($x = 0.2$ and 0.3) samples, while the sign of the Seebeck coefficient is negative for all the compounds. For $x = 0.075$, the Seebeck coefficient increases in absolute magnitude and saturates around -350 μV/K above 200 K, and the behavior for $x = 0.14$ and 0.17 is similar to $x = 0.075$ compound. As displayed in Fig. 2(b), the temperature dependence of the resistivity for these samples is well described with the VRH model. In the temperature region where charge transport is governed by VRH, the Seebeck coefficient should follow the relation,[12]

$$S(T) \propto T^{-1/4}. \qquad (3)$$

As shown in Fig. 3(b), the Seebeck coefficient of insulating materials in the low-temperature region is in good accord with this relation. The temperatures below which VRH conduction is observed are almost the same as those in the resistivity shown in Fig. 2(b). On the other hand, for the metallic samples, the absolute value of the Seebeck coefficient is much smaller than those of the insulating samples, increasing monotonically with increasing temperature, becoming about -50 and -40 μV/K at 300 K for $x = 0.2$ and 0.3, respectively. These values are definitely smaller than those of insulating samples, but relatively large for a metal. Because the Seebeck coefficient is less sensitive to the tiny amount of impurity phase than the resistivity, the large difference between the samples with $x \leqslant 0.17$ and $x \geqslant 0.2$ indicates that the insulator-metal transition observed in the resistivity measurement [see Fig. 2(a)] is of bulk intrinsic nature. We summarize the filling dependence of the conductivity at 2 K and the Seebeck coefficient at 300 K across the transition in Fig. 4(a). The x dependence of T_{VRH} is shown in Fig. 4(b). With increasing x, the VRH conduction is observed in the lower temperature region, signaling the approach to the metallic phase.

C. Magnetization and specific heat

Figure 5(a) shows the magnetization (M) as a function of temperature for $x = 0.2$ and 0.3. For $x = 0.2$, the increase
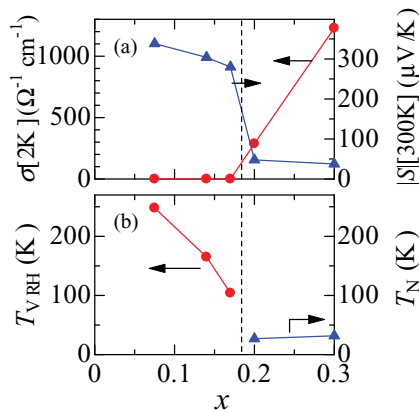
FIG. 4. (Color online) Doping dependence of several physical properties. (a) The x dependence of the electrical conductivity ($\sigma = 1/\rho$) at 2 K and Seebeck coefficient at 300 K. Insulator-metal transition takes place at around $x = 0.17$–0.2. (b) The x dependence of T_{VRH} (red circles) for $x = 0.075$, 0.14, and 0.17. T_N of Mn spin (blue triangles) is also plotted for the metallic compounds $x = 0.2$ and 0.3. Solid lines are merely guides to the eyes.

of magnetization is observed around 320 K, which is also discerned for insulating samples ($x = 0.075$, 0.14, and 0.17). Since the onset temperature of this increase in magnetization does not vary with the change in x and the possible impurity MnAs is known to be a ferromagnet with $T_c = 320$ K, this magnetic transition is not an intrinsic property of SmMnAsO$_{1-x}$, but should be ascribed to a tiny amount of impurity phase (MnAs).

Figures 5(b) and 5(c) show the magnetic-field (H) dependence of magnetization for $x = 0.2$ and 0.3. For $x = 0.2$, the H dependence is linear above 350 K, but below 300 K, a spontaneous moment due to the ferromagnetic impurity MnAs is observed below 1 T. For $x = 0.3$, the magnetization is almost linear in magnetic field in all the temperature region except for
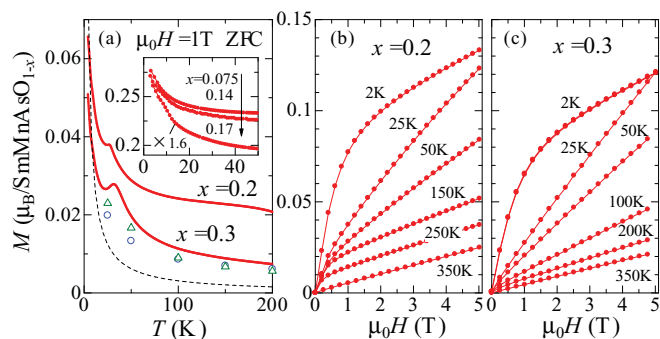
2 K. At 2 K, the magnetization for $x = 0.2$ and 0.3 shows nonlinear H dependence, which should be attributed to the tiny amount of unknown Curie spins.

Despite the presence of ferromagnetic component [see Figs. 5(b) and 5(c)], the linear slopes in the high-H region are considered to represent the intrinsic susceptibilities of $x = 0.2$ and 0.3. The intrinsic magnetizations at 1 T are estimated from this high-H linear portion above 25 K and plotted in Fig. 5(a) with the open circles and triangles, respectively. The estimated magnetizations of these compounds are almost identical above 100 K and increase with decreasing temperature. A dashed line indicates Curie contribution (C/T) from Sm^{3+}, which is estimated from the magnetization of SmZnAsO synthesized with the same procedure using the high-pressure synthesis technique. The temperature dependence of the magnetization for $x = 0.2$ and 0.3 appears almost parallel with this Curie contribution above 50 K, indicating the dominant contribution of Sm^{3+} f moments to the magnetic susceptibility. The positive offset from the magnetization of SmZnAsO is the contribution of Mn spins, which seems to be almost independent of temperature.

In the M-T curves shown in Fig. 5(a), peak structures are observed around 30 K for both metallic $x = 0.2$ and 0.3, while no anomalies are discerned for the insulating $x = 0.075$, 0.14, and 0.17 compounds around the corresponding temperatures as shown in the inset of Fig. 5(a). Below these anomalies, the magnetization slightly decreases, but increases again with decreasing temperature. This transition corresponds to the antiferromangetic or SDW order of Mn spins. The values of T_N for $x = 0.2$ and 0.3, plotted in Fig. 4(b), do not differ very much from each other, and there appears to be an antiferromagnetic metallic phase prevailing next to the antiferromagnetic insulating phase. The wide range of antiferromagnetic metal phase is similar to the case of NiS$_{2-x}$Se$_x$.[13] On the other hand, since LaMnPO and NdMnAsO are antiferromagnets with $T_N > 375$ K (see Ref. 5) and $T_N = 359$ K,[10] respectively, SmMnAsO is likely to be an antiferromagnetic insulator with such a high T_N. No clear magnetic transition was observed for $x = 0.075$ in the temperature range 300–400 K, suggesting that the T_N of SmMnAsO may be even higher than 400 K.

In Fig. 6, we show the specific heat (C_p) in the low-temperature region without magnetic field for $x = 0.075$, 0.2, and 0.3. The peak structures are observed around 4 K for all the samples. These anomalies are ascribed to the magnetic transitions of Sm^{3+} f moments. A similar peak structure was also observed around 4–5 K in SmFeAs(O$_{1-x}$F$_x$)[14,15] and was interpreted as resulting from the antiferromagnetic transition of Sm^{3+} f moments on the basis of the comparison with the antiferromagneitc transition in Sm$_2$CuO$_4$ at $T_N = 5.9$ K.[16] For the present $x = 0.2$ and 0.3, the specific heat begins to increase below 3 K with decreasing temperature. This probably originates from the SmAs impurity, as it has been reported to show the peak structure at 2 K in literature.[17] This assumption is consistent with the absence of the upturn below 3 K in the $x = 0.075$ compound, which does not contain SmAs.

The specific heat generally consists of the contributions from conduction electrons (C_{el}), phonons (C_{ph}), and magnetic excitations (C_{mg}). C_{el} and C_{ph} are expressed as $C_{\mathrm{el}} = \gamma T$

FIG. 5. (Color online) (a) Temperature (T) dependence of the magnetization (M) for $x = 0.2$ and 0.3. Open circles and triangles indicate the intrinsic magnetization values of $x = 0.2$ and 0.3 estimated from the slopes of the linear parts of the isothermal M-H curves [(b) and (c)], respectively. The detailed procedure of the estimation is described in the text. The inset shows the temperature dependence of the magnetization below 50 K for the insulating compounds with $x = 0.075$, 0.14, and 0.17. (b) and (c) Magnetic field (H) dependence of the magnetization (M) for (b) $x = 0.2$ and (c) 0.3 at several temperatures.
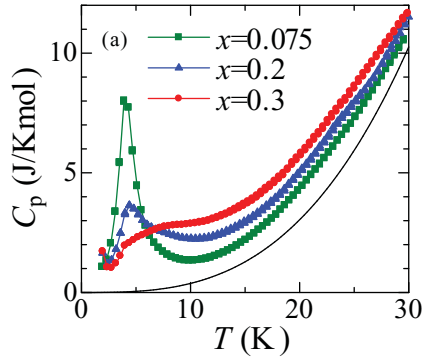
FIG. 6. (Color online) (a) Temperature (T) dependence of specific heat (C_p) for $x = 0.075$, 0.2, and 0.3 below 30 K. The solid line indicates the phonon specific heat (βT^3).

and $C_{ph} = \beta T^3$ at the low temperatures, where γ and β are electronic and phonon specific-heat coefficients, respectively. As for the value of β, it is useful to refer to the result ($\beta \sim 0.36$ mJ/mol K^4) of SmFeAs(O$_{1-x}$F$_x$) with the same structure.[14,15] We estimate the C_{mg} of Sm^{3+} f moments for $x = 0.075$ by $(C_p - \beta T^3)/T$ and calculate the corresponding entropy. The entropy shows a sharp increase around 4 K and gradually approaches to $R \ln 2$, similarly to the case of SmFeAs(O$_{1-x}$F$_x$). As x is increased, the peak structure of C_p becomes smaller, and the magnetic contribution of Sm^{3+} f moments seems to be present up to the higher temperatures. Although the Mn spins order antiferromagnetically around 27 K for $x = 0.2$ as described above, the corresponding anomaly is quite small, clearly indicating the itinerant nature of the Mn magnetism for $x \geqslant 0.2$. The determination of the genuine value of γ was difficult for the present samples due to the large magnetic contribution of Sm^{3+} f moments.

D. Hall coefficient and magnetoresistance

In order to obtain the information on the Fermi surface in the metallic samples ($x = 0.2$ and 0.3), we measured the Hall resistivity ρ_{yx} [see Figs. 7(a) and 7(b)]. The slope of the Hall resistivity is negative both for $x = 0.2$ and 0.3, and almost linear with magnetic field above T_N. In this temperature region, the Hall coefficient gradually increases in absolute magnitude as the temperature is decreased, as plotted in Fig. 7(c). The
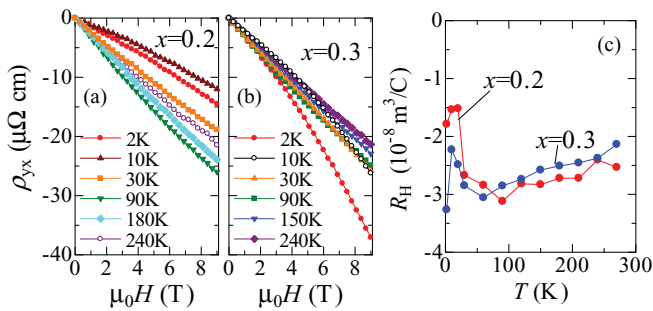
observed absolute value of the Hall coefficient is one order of magnitude larger than that expected from the nominal oxygen deficiency. This fact can be accounted for in terms of the existence of the hole-type Fermi surface in addition to the electron type one in the metallic phase derived from the Mott insulator, where a dramatic reconstruction of the band structure is expected. According to the band calculation for RFeAsO,[18–21] the multiband structure consisting of five Fe-3d bands is suggested near the Fermi energy and there seem to be both electron and hole pockets at the Fermi surfaces. Although the band calculation has not been performed for the metallic SmMnAsO$_{1-x}$, the complex multiband structure is inferred as well from the present result of Hall coefficient.

The magnitude of the slope of the ρ_{yx} versus H curve in the low-field region begins to decrease at 30 K both for $x = 0.2$ and 0.3. Since the antiferromagnetic transition occurs around 30 K, the decrease of the absolute value of Hall coefficient (R_H) should be related with the change in the electronic structure. However, the absolute magnitude of R_H usually increases below the antiferromagnetic transition because the Fermi surface shrinks and the carrier density decreases.[13,22] Again, the complex multiband structure of Mn-3d bands around the Fermi energy would be the origin for the apparent decrease in the absolute magnitude of the Hall coefficient. The R_H in the presence of both electron- and hole-type carriers is generally expressed as[23]

$$R_H = \frac{1}{e} \frac{(n_h \mu_h^2 - n_e \mu_e^2) + \mu_e^2 \mu_h^2 (n_h - n_e)(\mu_0 H)^2}{(\mu_e n_e + \mu_h n_h)^2 + \mu_e^2 \mu_h^2 (n_h - n_e)^2 (\mu_0 H)^2}, \quad (4)$$

where n_e (n_h) and μ_e (μ_h) are the density and mobility of electron (hole), respectively. The H^2 term in Eq. (4) is significant only in the low-temperature regions of good metals with high mobility, which should be far from the present case with substantial disorders and hence with poor mobility. Therefore, we can safely use the formula in the low-field limit, $R_H = e^{-1}(n_h \mu_h^2 - n_e \mu_e^2)/(n_e \mu_e + n_h \mu_h)^2$. Upon the SDW transition, a gap is likely to open at the electron-type Fermi surface, which decreases n_e and hence the magnitude of negative R_H for $x = 0.2$. The Hall resistivity ρ_{yx} shows convex upward curvature below T_N. This behavior is ascribed to the field-induced change of electronic structure or related parameters (n_e, μ_e, n_h, and μ_h), which also manifests itself as the unconventional large positive magnetoresistance as described in the following.

Figures 8(a) and 8(b) show the temperature dependence of the resistivity in several magnetic fields up to 9 T for $x = 0.2$ and 0.3, respectively. In both compounds, an unexpectedly large positive magnetoresistance effect is observed in a wide range of temperature and its magnitude increases with decreasing temperature. The triangles in Figs. 8(a) and 8(b) indicate the values of T_N in magnetic fields, which are determined from the magnetization data. The T_N value slightly decreases both for $x = 0.2$ and 0.3 as the magnetic field is increased. For $x = 0.2$, the resistivity shows an upturn below a temperature slightly above T_N in zero field, and the temperature of the resistivity minimum increases with increase in the magnetic field. For $x = 0.3$, the resistivity monotonically decreases down to the lowest temperature in zero field, and the temperature-dependence is proportional to
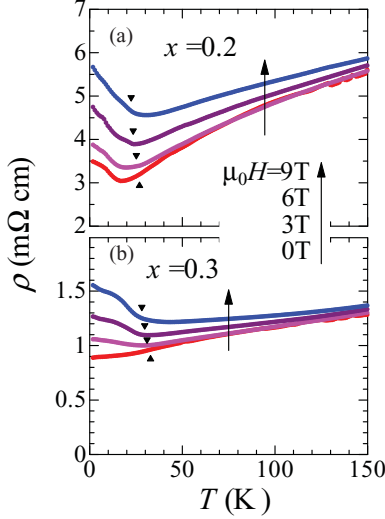

FIG. 7. (Color online) (a) and (b) Magnetic field (H) dependence of Hall resistivity for (a) $x = 0.2$ and (b) 0.3. The contribution arising from the magnetoresistance of the longitudinal resistivity is eliminated by using the Hall voltage values at $\pm H$. (c) Temperature (T) dependence of the Hall coefficient ($\equiv R_H$).

FIG. 8. (Color online) (a) and (b) Temperature (T) dependence of resistivity (ρ) for (a) $x = 0.2$ and (b) $x = 0.3$ in various magnetic fields. The triangles indicate the T_N determined from the magnetization data.

T^2 below 25 K. In magnetic fields above 3 T, the resistivity upturn becomes visible below T_N.

In Figs. 9(a) and 9(b), we show the field dependence of the magnetoresistance magnitude $\{[\rho(H) - \rho(H = 0)]/\rho(H = 0)\}$. The magnetoresistance magnitude is almost proportional to $H^{1.5}$ up to 9 T both for $x = 0.2$ and 0.3 at all the temperatures, as exemplified by the solid curves in Figs. 9(a) and 9(b). We have tried the Kohler's plot (not shown), but these magnetoresistance data at several temperatures from 2 to 200 K do not collapse on a single curve either for $x = 0.2$ or 0.3. Usually, a violation of the Kohler's rule indicates that the scattering rates for electron- and hole-type carriers are different and/or that the scattering rates are nonuniform over the Fermi surface. In the present case, however, this should be interpreted as an indication of different mechanism(s) of magnetoresistance from the bending of electron orbitals. In Fig. 9(c), the magnetoresistance magnitude at 9 T is plotted against temperature. The magnetoresistance shows a maximum at 20 K (slightly below T_N) for $x = 0.2$, while it increases monotonically down to the lowest temperature for $x = 0.3$. The magnitude of the magnetoresistance seems to be little dependent on the value
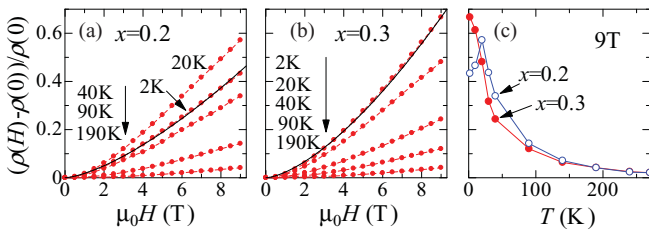

FIG. 9. (Color online) Isothermal magnetoresistance magnitude $\{\equiv [\rho(H) - \rho(0)]/\rho(0)\}$ for (a) $x = 0.2$ and (b) $x = 0.3$ at various temperatures. The solid lines indicate the power-low dependence of $H^{1.5}$. (c) Temperature (T) dependence of the (longitudinal) magnetoresistance magnitude at 9 T for $x = 0.2$ (open circles) and 0.3 (closed circles).

of x above T_N, reaches more than 50% at the maximum, and persists to high temperatures, e.g., 5% even at 190 K.

As possible origins of such large magnetoresistance, we may consider the following five mechanisms: (i) grain-boundary scattering, (ii) weak localization, (iii) spin scattering, (iv) Lorentz force, and (v) changes in the carrier density and/or the mobility associated with the change in the band structure. The mechanism (v) would be most plausible as the origin for the large positive magnetoresistance, although we cannot uniquely identify the origin. In the following, we briefly discuss these mechanisms one by one: (i) the large negative magnetoresistance associated with the spin-polarized intergrain tunneling is observed at low temperatures in a polycrystalline ferromagnetic metal of $La_{2/3}Sr_{1/3}MnO_3$.[24] Apart from the sign, the temperature dependence shown in Fig. 9(c) is reminiscent of this intergrain-tunneling magnetoresistance. However, $SmMnAsO_{1-x}$ is antiferromagnetic and the tunneling process should not be affected by the relative angle of the spin directions of the neighboring grains. Indeed, similar positive magnetoresistance has been observed both for single crystal and polycrystalline samples of antiferromagnetic RFeAsO.[25–27]

(ii) The upturn of the resistivity in the zero field for $x = 0.2$ may be related with the weak-localization effect. In that case, the field effect on the localization would manifest the magnetoresistance. However, as shown in Figs. 9(a) and 9(b), the $H^{1.5}$ dependence of the magnetoresistance magnitude is clearly different from $H^{0.5}$ or $\ln H$ behavior expected for weak localization, and does not change across the temperature of the resistivity upturn. Therefore, the weak localization should be irrelevant to the observed magnetoresistance effect.

(iii) In view of the fact that the magnetoresistance magnitude takes a maximum around T_N for $x = 0.2$, the magnetoresistance would be somehow related with the antiferromagnetic transition of Mn spins. The field suppression of the spin scattering is known to be a major source of the magnetoresistance in magnetic metals, but it usually causes a negative magnetoresistance effect,[28] as observed in the SDW states of metallic $V_{2-y}O_3$.[29]

(iv) Positive magnetoresistance is generally caused by the Lorentz force.[30] The magnetoresistance in the presence of both electron- and hole-types carriers is expressed as[31]

$$\frac{\rho(H) - \rho(0)}{\rho(0)} = \frac{n_e n_h \mu_e \mu_h (\mu_e - \mu_h)^2 (\mu_0 H)^2}{(n_e \mu_e + n_h \mu_h)^2 + (\mu_0 H)^2 (\mu_e \mu_h n_h + \mu_h \mu_e n_e)^2}.$$

(5)

The $H^{1.5}$ dependence of the magnetoresistance magnitude might be viewed as close to the H^2 dependence represented by Eq. (5). However, the magnitude of the magnetoresistance induced by the Lorentz force is usually as small as a few percent, except for metals with very high mobility. The present materials are strongly correlated metals derived from a Mott insulator, and also contain substantial disorder. Therefore, it would be unlikely that the Lorentz force gives rise to such a gigantic magnetoresistance as exceeding 50%.

(v) Similar positive magnetoresistance effect as large as several tens of percent has been reported in SDW states of poly and single-crystalline RFeAsO[25–27] and single-crystalline $SrFe_2As_2$.[32] For the present $SmMnAsO_{1-x}$, as inferred from the Hall-effect data, a gap opening on the electron Fermi

surface takes place upon the SDW transition. Also, the slope of the Hall resistivity becomes large as the field is increased, as shown in Figs. 7(a) and 7(b). Considering the relation $R_H = e^{-1}(n_h\mu_h^2 - n_e\mu_e^2)/(n_e\mu_e + n_h\mu_h)^2$, this observation indicates the increase in n_e and/or μ_e, or the decrease in n_h and/or μ_h. Although the mechanism is not clear at present, if the n_h and/or μ_h is reduced by the application of the magnetic field, then the positive magnetoresistance as well as the field dependence of the Hall resistivity can be explained in a consistent manner. This situation reminds us of the case of ferromagnetic (Fe,Co)Si,[33] where the large positive magnetoresistance effect was observed in the low-temperature region. In this case, the Zeeman shift of exchange-split bands decreases the carrier density in the minority band, leading to the increase of the total resistivity, provided that the mobility of the minority-spin band is larger than that of the majority-spin band. In the case of SmMnAsO$_{1-x}$, electron- and hole-type carriers might play a similar role to the case of majority- and minority-spin bands, respectively, and the change in the Fermi surface as affected also by the Zeeman splitting would be important. However, the situation in the present case is more complex than in the (Fe,Co)Si case, due to the presence of four kinds of carriers, i.e., electron- and hole-type carriers with up and down spin, this makes the quantitative analysis difficult.

IV. CONCLUSIONS

We synthesized a series of SmMnAsO$_{1-x}$ with controlled electron-doping level by using a high-pressure synthesis technique. We showed that, as the electron doping is increased with increasing oxygen deficiency, the resistivity decreases monotonically, and the insulator-metal transition occurs between $x = 0.17$ and 0.2. The temperature dependence of the Seebeck coefficient is largely different between $x \leqslant 0.17$ and $x \geqslant 0.2$, confirming the insulator-metal transition of bulk nature in accord with the resistivity measurement. The metallic $x = 0.2$ and 0.3 compounds show the antiferromagnetic order at low temperatures below 30 K. Upon the antiferromagnetic or SDW transition, the metallic compounds show a reduction in the magnitude of Hall coefficient (with negative sign) in a low-field region, indicating the coexistence of electron- and hole-type carriers as well as the gap opening on the electron-type Fermi surface. Both the $x = 0.2$ and 0.3 compounds show an unusually large positive magnetoresistance effect in a wide range of temperatures, which exceeds 50% at 2 K. We attribute the observed magnetoresistance effect also to the field-induced change in the band structure consisting of complex multiple Fermi surfaces.

[1] Y. Kamihara, T. Watanabe, M. Hirano, and H. Hosono, J. Am. Chem. Soc. **130**, 3296 (2008).

[2] H. Takahashi, K. Igawa, K. Arii, Y. Kamihara, M. Hirano, and H. Hosono, Nature (London) **453**, 3296 (2008).

[3] T. C. Ozawa and S. M. Kauzlarich, Sci. Technol. Adv. Mater. **9**, 033003 (2008).

[4] H. Hosono, J. Phys. Soc. Jpn. Suppl. C **77**, 1 (2008).

[5] H. Yanagi, T. Watanabe, K. Kodama, S. Iikubo, S. Shamoto, T. Kamiya, M. Hirano, and H. Hosono, J. Appl. Phys. **105**, 093916 (2009).

[6] H. Yanagi, K. Fukuma, T. Kamiya, M. Hirano, and H. Hosono, Mater. Sci. Eng. B **173**, 47 (2010).

[7] K. Kayanuma, H. Hiramatsu, T. Kamiya, M. Hirano, and H. Hosono, J. Appl. Phys. **105**, 073903 (2009).

[8] K. Miyazawa, K. Kihou, P. M. Shirage, C.-H. Lee, H. Krro, H. Eisaki, and A. Iyo, J. Phys. Soc. Jpn. **78**, 034712 (2009).

[9] H. Ohta and K. Yoshimura, Phys. Rev. B **80**, 184409 (2009).

[10] A. Marcinkova, T. C. Hansen, C. Curfs, S. Margadonna, and J. W. G. Bos, Phys. Rev. B **82**, 174438 (2010).

[11] M. Imada, A. Fujimori, and Y. Tokura, Rev. Mod. Phys. **70**, 1039 (1998).

[12] R. Ang, W. J. Lu, R. L. Zhang, B. C. Zhao, X. B. Zhu, W. H. Song, and Y. P. Sun, Phys. Rev. B **72**, 184417 (2005).

[13] S. Miyasaka, H. Takagi, Y. Sekine, H. Takahashi, N. Môri, and R. Cava, J. Phys. Soc. Jpn. **69**, 3166 (2000).

[14] M. Tropeano, A. Martinelli, A. Palenzona, E. Bellingeri, E. Galleani d'Agliano, T. D. Nguyen, M. Affronte, and M. Putti, Phys. Rev. B **78**, 094518 (2008).

[15] S. Riggs, C. Tarantini, J. Jaroszynski, A. Gurevich, A. Palenzona, M. Putti, T. D. Nguyen, and M. Affronte, Phys. Rev. B **80**, 214404 (2009).

[16] S. Ghamaty, B. W. Lee, J. T. Markert, E. A. Early, T. Bjornholm, C. L. Seaman, and M. B. Maple, Physica C **160**, 217 (1989).

[17] R. B. Beeken and J. W. Schweitzer, Phys. Rev. B **19**, 5810 (1979).

[18] K. Kuroki, H. Usui, S. Onari, R. Arita, and H. Aoki, Phys. Rev. B **79**, 224511 (2009).

[19] I. I. Mazin, M. D. Johannes, L. Boeri, K. Koepernik, and D. J. Singh, Phys. Rev. B **78**, 085104 (2008).

[20] Z. P. Yin, S. Lebègue, M. J. Han, B. P. Neal, S. Y. Savrasov, and W. E. Pickett, Phys. Rev. Lett. **101**, 047001 (2008).

[21] S. Ishibashi, K. Terakura, and H. Hosono, J. Phys. Soc. Jpn. **77**, 053709 (2008).

[22] S. Ishida, M. Nakajima, Y. Tomioka, T. Ito, K. Miyazawa, H. Kito, C. H. Lee, M. Ishikado, S. Shamoto, A. Iyo, H. Eisaki, K. M. Kojima, and S. Uchida, Phys. Rev. B **81**, 094515 (2010).

[23] R. A. Smith, *Smiconductors* (Cambridge University Press, Cambridge, England, 1978).

[24] H. Y. Hwang, S.-W. Cheong, N. P. Ong, and B. Batlogg, Phys. Rev. Lett. **77**, 2041 (1996).

[25] J. Dong, H. J. Zhang, G. Xu, Z. Li, G. Li, W. Z. Hu, D. Wu, G. F. Chen, X. Dai, J. L. Luo, Z. Fang, and N. L. Wang, Europhys. Lett. **83**, 27006 (2008).

[26] M. A. McGuire, A. D. Christianson, A. S. Sefat, B. C. Sales, M. D. Lumsden, R. Jin, E. A. Payzant, D. Mandrus, Y. Luan, V. Keppens, V. Varadarajan, J. W. Brill, R. P. Hermann, M. T. Sougrati, F. Grandjean, and G. J. Long, Phys. Rev. B **78**, 094517 (2008).

[27] P. Cheng, H. Yang, Y. Jia, L. Fang, X. Zhu, G. Mu, and H-H. Wen, Phys. Rev. B **78**, 134508 (2008).

[28] K. Usami, J. Phys. Soc. Jpn. **45**, 466 (1978).

[29] S. Klimm, G. Gerstmeier, H. Paulin, M. Klemm, and S. Horn, Physica B **230-232**, 992 (1997).

[30] In our measurements when the magnetic field is parallel to the current, the resistivity should not be affected by the Lorentz force basically. However, if the electron flow is almost limited along the in-plane direction of randomly-oriented grains in polycrystalline $SmMnAsO_{1-x}$, the Lorentz force would cause the magnetoresistance.

[31] J. M. Ziman, *Principles of The Theory of Solids* (Cambridge University Press, Cambridge, England, 1979).

[32] G. F. Chen, Z. Li, J. Dong, G. Li, W. Z. Hu, X. D. Zhang, X. H. Song, P. Zheng, N. L. Wang, and J. L. Luo, Phys. Rev. B **78**, 224512 (2008).

[33] Y. Onose, N. Takeshita, C. Terakura, H. Takagi, and Y. Tokura, Phys. Rev. B **72**, 224431 (2005).

[34] T. Okuda, K. Nakanishi, S. Miyasaka, and Y. Tokura, Phys. Rev. B **63**, 113104 (2001).

[35] N. W. Ashcroft and N. D. Mermin, *Solid State Physics* (Thomson Learning, 1976).